High energy neutrino signals of four neutrino mixing

Sharada Iyer Dutta[1], Mary Hall Reno[2] and Ina Sarcevic[1]
[1]*Department of Physics, University of Arizona, Tucson, Arizona 85721*
[2]*Department of Physics and Astronomy, University of Iowa, Iowa City, Iowa 52242*

We evaluate the upward shower and muon event rates for two characteristic four neutrino mixing models for extragalactic neutrinos, as well as for the atmospheric neutrinos, with energy thresholds of 1 TeV, 10 TeV and 100 TeV. We show that by comparing the shower to muon event rates, one can distinguish between oscillation and no-oscillation models. By measuring shower and muon event rates for energy thresholds of 10 TeV and 100 TeV, and by considering their ratio, it is possible to use extragalactic neutrino sources to determine the type of four-flavor mixing pattern. We find that over several years of data taking, a kilometer-size detector has a very good chance of providing valuable information about the physics beyond the Standard Model.

I. INTRODUCTION

The combined results of solar, atmospheric and laboratory experiments with neutrinos, taken at face value, require a fourth neutrino species. This follows from the observation that the results of the three categories of experiments require at least three mass-squared differences δm^2. The mass-squared difference for solar neutrino experiments is limited to $\delta m^2_{solar} \lesssim 10^{-3}$ eV^2 [1]. The SuperKamiokande results [2] for atmospheric neutrinos require $\delta m^2_{atm} \sim 3 \times 10^{-3}$ eV^2, and the laboratory LSND experiment [3] limits $\delta m^2_{LSND} > 0.2$ eV^2. While precision measurements of the invisible decay width of the Z^0 boson constrain the addition of a fourth generation neutrino species with weak interactions, they do not constrain the possibility of a sterile neutrino species mixing with the ordinary electron, muon and tau neutrinos. Analyses of solar and atmospheric experiments assuming pure $\nu_i \to \nu_s$ oscillations indicate that the data do not support the hypothesis, however, combined fits to all of the experimental data do require a sterile neutrino species [4].

Recent SuperK data on atmospheric neutrinos indicate $\nu_\mu \to \nu_\tau$ oscillations with mixing being nearly bi-maximal [2]. We have shown in Ref. [5] that for extragalactic sources of muon neutrinos, mixing with tau neutrinos in transit to the Earth leads to distinct signatures of oscillation which do not require explicit identification of a tau lepton in large underground experiments. In this paper, we investigate the signatures of neutrino oscillations in large underground experiments for models with three active neutrinos and one sterile neutrino whose mixing is constrained by lower energy experiments.

II. MIXING MODELS AND EXTRAGALACTIC FLUXES

Global fits to oscillation data fall into two distinct patterns of neutrino mixing. The first is a mass spectrum in which $\nu_e \leftrightarrow \nu_s$ with a mass splitting δm^2_{solar}, $\nu_\mu \leftrightarrow \nu_\tau$ with δm^2_{atm} and a splitting between the two nearly degenerate pairs characterized by δm^2_{LSND}. The approximate mixing matrix in this scenario has the form [4]

$$\begin{pmatrix} \nu_s \\ \nu_e \\ \nu_\mu \\ \nu_\tau \end{pmatrix} = \begin{pmatrix} \frac{1}{\sqrt{2}} & \frac{1}{\sqrt{2}} & 0 & 0 \\ -\frac{1}{\sqrt{2}} & \frac{1}{\sqrt{2}} & \epsilon & \epsilon \\ \epsilon & -\epsilon & \frac{1}{\sqrt{2}} & \frac{1}{\sqrt{2}} \\ 0 & 0 & -\frac{1}{\sqrt{2}} & \frac{1}{\sqrt{2}} \end{pmatrix} \begin{pmatrix} \nu_0 \\ \nu_2 \\ \nu_2 \\ \nu_3 \end{pmatrix} , \quad (1)$$

where $\epsilon < 0.1$ [4]. Following Ref. [4], we call this a $2+2$ scenario.

The second pattern of neutrino mass and mixing, allowed by the most recent analysis of the LSND experiment, has large mixing between the three ordinary neutrinos and a small mixing with the sterile neutrino, characterized by small parameters ϵ and δ. A characteristic mixing matrix has the form [4]

$$\begin{pmatrix} \nu_s \\ \nu_e \\ \nu_\mu \\ \nu_\tau \end{pmatrix} = \begin{pmatrix} 1 & \frac{\delta}{2} - \frac{\epsilon}{\sqrt{2}} & -\frac{\delta}{2} - \frac{\epsilon}{\sqrt{2}} & -\frac{\delta}{\sqrt{2}} \\ \epsilon & \frac{1}{\sqrt{2}} & \frac{1}{\sqrt{2}} & 0 \\ \delta & -\frac{1}{2} & \frac{1}{2} & \frac{1}{\sqrt{2}} \\ 0 & \frac{1}{2} & -\frac{1}{2} & \frac{1}{\sqrt{2}} \end{pmatrix} \begin{pmatrix} \nu_0 \\ \nu_2 \\ \nu_2 \\ \nu_3 \end{pmatrix} . \quad (2)$$

Following Ref. [4], we call this a $1+3$ scenario.

For extragalactic sources, because of the large distances involved, the oscillation flavor ratios are essentially independent of mass-squared differences and neutrino energy, since

$$\langle \sin^2 \left(\frac{1.27 \delta m^2 L}{E} \right) \rangle \simeq \frac{1}{2} , \quad (3)$$

for δm^2 in eV^2, L in km, and E in GeV. Consequently, the oscillation probabilities can be written as

$$P(\nu'_\ell \to \nu_\ell) = \sum_j \mid U_{\ell j} \mid^2 \mid U_{\ell' j} \mid^2 , \quad (4)$$

in terms of the elements of the neutrino mixing matrix $U_{\ell j}$. The ν_ℓ flux in detectors F^D_ℓ, in terms of the fluxes at the source F^S_ℓ are [6,7]

$$F^D_{\nu_\ell} = \sum_{\ell'} P(\nu'_\ell \to \nu_\ell) F^S_{\nu_{\ell'}} \ . \qquad (5)$$

As we discuss below, our "source" fluxes are actually summed over many sources to yield isotropic fluxes. We continue to denote these isotropic fluxes, unmodified by oscillations, as the source fluxes.

Given source ratios of fluxes $\nu_s^S : \nu_e^S : \nu_\mu^S : \nu_\tau^S = 0 : 1 : 2 : 0$ yield different ratios of neutrino fluxes at the detector, depending on whether the 2+2 or 1+3 scenario describes four-neutrino mixing. In the $1 + 3$ case with small ϵ and δ, the detector ratios are approximately $0 : 1 : 1 : 1$, while for the $2 + 2$ case, sterile neutrinos make an important component of the flux at the Earth, with $\nu_s^D : \nu_e^D : \nu_\mu^D : \nu_\tau^D \simeq 0.5 : 0.5 : 1 : 1$. With three neutrino species and bi-maximal mixing, one finds $\nu_e^D : \nu_\mu^D : \nu_\tau^D \simeq 1 : 1 : 1$. Without mixing, the source fluxes and detector fluxes have the same flavor ratios of $1 : 2 : 0$. As a result, the $1 + 3$ scenarios essentially reproduce the three-flavor bi-maximal mixing scenario, while the $2 + 2$ scenarios lie between the 3-flavor bi-maximal mixing model and the no-mixing model.

There are a variety of predictions for isotropic neutrino fluxes from active galactic nuclei (AGN), gamma ray bursters (GRB) and models with topological defects. A sample of these predictions for muon neutrino plus antineutrino fluxes, in the absence of oscillations, are shown in Fig. 1. These include the AGN models of Stecker and Salamon (AGN_SS) [8] and of Mannheim Model A (AGN_M95) [9]. Both of these models predict neutrinos fluxes that represent the upper bounds for their class of the models. In particular, the Stecker-Salamon flux is an upper bound for AGN core emission, while Mannheim Model A is an upper bound for AGN jet emission models. The Stecker-Salamon flux is bound by the the diffuse X-ray background, while Mannheim flux is bound by the extragalactic gamma ray background. GRB predictions are represented by the Waxman-Bahcall model of Ref. [10] (GRB_WB). Two topological defect models, from Sigl, Lee, Schramm and Coppi (TD_SLSC) [11] and Wichoski, MacGibbon and Brandenberger (TD_WMB) [12] are also shown. We include fluxes with energy behaviors like $1/E$ and $1/E^2$ as well. We chose normalization for each of these fluxes consistent with the current limits [13], $F^S_{\nu_\mu} = 10^{-12}\ (E/\mathrm{GeV})^{-1}\mathrm{GeV}^{-1}\mathrm{cm}^{-2}\mathrm{sr}^{-1}\mathrm{s}^{-1}$ and $F^S_{\nu_\mu} = 10^{-6}\ (E/\mathrm{GeV})^{-2}\mathrm{GeV}^{-1}\mathrm{cm}^{-2}\mathrm{sr}^{-1}\mathrm{s}^{-1}$ (in which the fluxes include neutrinos and antineutrinos in equal amounts and correspond to the initial fluxes before accounting for oscillations). Our choice of normalization for E^{-2} flux is a factor of ten larger than recently proposed neutrino flux associated with GRB ($F^S_{\nu_\mu} = 10^{-7}\ (E/\mathrm{GeV})^{-2}\mathrm{GeV}^{-1}\mathrm{cm}^{-2}\mathrm{sr}^{-1}\mathrm{s}^{-1}$) [14], and a factor of 50 larger than the upper bound for strong source evolution previously discussed by Waxman and Bahcall [15]. The E^{-1} flux is smoothly cut off at high energies, as indicated in Fig. 1.

Although the normalizations of the fluxes of neutrinos from astrophysical sources are uncertain, we evaluate event rates quantitatively for these representative energy behaviors of the fluxes which, as models improve, can be rescaled to accommodate different normalizations.

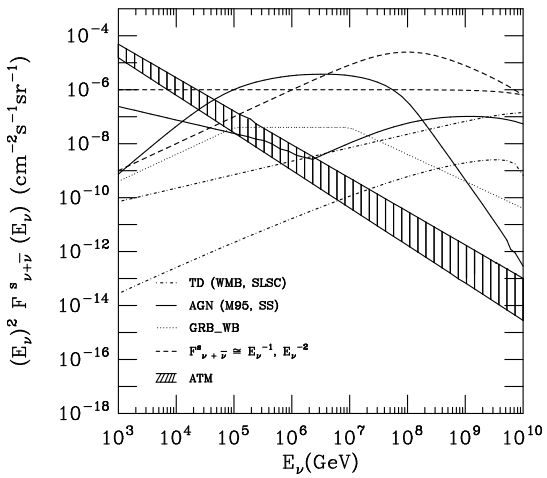

FIG. 1. Isotropic muon neutrino plus antineutrino flux predictions for AGN models (solid lines, upper curve at low energy corresponds to AGN_M95, while the lower curve is for AGN_SS model), GRB (dotted line), topological defects models (dash-dotted lines, upper curve corresponds to TD_(Model A) WMB, while the lower curve is for TD_SLSC), E^{-1} flux (lower dashed line at low energy) and E^{-2} (upper dashed line at low energy) and angle-dependent atmospheric (ATM). The flux is scaled by neutrino energy squared and the antineutrino flux is taken equal to the neutrino flux.

For comparison, the hatched curve shows the angle dependent atmospheric flux (ATM) [16] from kaon and pion decays (conventional flux). We have extrapolated this flux beyond the 10 TeV range given in Ref. [16] using an angular dependent power law. This does not account for the change in the input cosmic ray spectrum, the so-called "knee" at energies of $\sim 10^6$ GeV [17], which translates to a reduced conventional neutrino flux at high energies. Thus, we overestimate the conventional neutrino event rates, especially at our highest threshold of 100 TeV, however, at that threshold, the atmospheric rates are small. Our evaluation does not include the prompt neutrino flux from semileptonic decays of charmed particles produced in the atmosphere, which result in neutrino fluxes with a power law increased by one factor of energy. Recent evaluations of the prompt neutrino flux suggest that it is important only above 100 TeV [18–20], although it has been emphasized that there are large theoretical uncertainties in the evaluation [21].

In our previous work [5], we have evaluated how neutrino interactions in the Earth modify these representative neutrino fluxes with the regeneration attributed to the neutral current interactions. In addition, for tau neutrinos, we described the extent to which neutral current

interactions and charged current production of τ followed by its decay, regenerate neutrinos. There, we made a detailed numerical evaluation of the "pile-up" of tau neutrinos that was discussed by Halzen and Saltzberg in Ref. [22]. In the next section, we use the neutrino fluxes of Fig. 1 modified due to their passage through the Earth [5] in the appropriate flavor proportions for the $1+3$ and $2+2$ scenarios.

III. UNDERGROUND SIGNATURES

Backgrounds from atmospheric muons make downward event rates difficult to extract, so our focus is on upward events. Two types of events will be produced: muon events and shower events. The muon events come from upward muons from $\nu_\mu \to \mu$ charged current events and from charged current production of taus followed by a muonic decay, $\nu_\tau \to \tau \to \mu X$. In spite of the pile-up in the tau neutrino flux, the net effect of oscillations is to reduce the muonic event rate by approximately a factor of two relative to the no-oscillation rate, whether in the $1+3$ or $2+2$ mixing scenario. Given the uncertainties in the normalizations of the extragalactic fluxes (unlike the atmospheric flux), the muon event rate is not enough to distinguish oscillation scenarios from no-oscillation scenarios.

The distinction between oscillation and no-oscillation scenarios comes by comparing the muon rate with the shower rate. The principle of this procedure is very similar to what some experiments will be able to do with low energy neutrinos: namely, to compare the neutral current rate to the charge current interaction rate. In large neutrino telescopes, tau identification is difficult, and we assume that showers of hadronic and electromagnetic origin cannot be distinguished. Consequently, the shower rate comes from the following processes from neutrino-nucleon (N) interactions:

$$\begin{gathered}\nu_\tau N \to \tau + \text{hadrons},\ \tau \to \nu_\tau + \text{hadrons}\ , \\ \nu_\tau N \to \tau + \text{hadrons},\ \tau \to \nu_\tau + e + \nu_e\ , \\ \nu_\tau N \to \nu_\tau + \text{hadrons}, \\ \nu_{e,\mu} N \to \nu_{e,\mu} + \text{hadrons}, \\ \nu_e N \to e + \text{hadrons}\ .\end{gathered} \tag{6}$$

The shower energy is taken as the sum of hadronic and electron energies including both the production vertex and the decay vertex, where applicable.

The upward muon rates are determined from an evaluation of the quantity

$$\begin{aligned}\text{Rate}= AN_A \int_{E_\mu^{\min}} dE_\nu \int dy \int dz \langle R_\mu(E_\mu, E_\mu^{\min})\rangle \frac{d\sigma_{cc}}{dy} \\ \times F_\nu(E_\nu, X)\Theta(E_\mu - E_\mu^{\min})\, f_\mu(E_\nu, y, z)\end{aligned} \tag{7}$$

where $E_\mu = E_\nu(1-y)z$. The function f depends whether the source of the muons is muon neutrino charged current interactions or tau neutrino charged current interactions followed by the muonic decay of the tau:

$$\begin{aligned} f_\mu(E_\nu, y, z) &= \delta(1-z) \text{ for } \nu_\mu \to \mu\ , \\ f_\mu(E_\nu, y, z) &= \frac{dn(E_\mu)}{dz} \text{ for } \nu_\tau \to \tau \to \mu\ , \end{aligned} \tag{8}$$

where the decay formula appears in the appendix of Ref. [5]. The quantity A is the effective area (taken as 1 km^2 here), N_A is Avogadro's number and the differential cross section is for neutrino-interactions. The average range of the muon $\langle R\rangle$ [23], for initial energy E_μ and final energy $E_\mu^{\min}$ is the additional space dimension that makes up the target volume. The column depth (X) dependence of the neutrino flux represents the angular dependence of the flux due to the attenuation of the flux after passage through the Earth, and in the case of atmospheric neutrinos, includes the angular dependence of the flux at the surface of the Earth.

For the shower rate, one does not have the benefit of the muon range, so the full instrumented volume V enters into the calculation of the event rate, here taken to be 1 km^3:

$$\begin{aligned}\text{Rate}= VN_A \int_{E_{\rm shr}^{\min}} dE_\nu \int dy \int dz \frac{d\sigma}{dy} \\ \times F_\nu(E_\nu, X)\Theta(E_{\rm shr} - E_{\rm shr}^{\min})\, f_s(E_\nu, y, z)\ ,\end{aligned} \tag{9}$$

where f_s has a similar form to f_μ. Details of the differential decay distribution of the tau used in the evaluation, as well as the specific dependence of $E_{\rm shr}$ on E_ν, y and z appear in [5]. The differential cross section is either charged current or neutral current, depending on which process in Eq. (6) is being considered.

The neutrino and antineutrino cross sections [24] are evaluated using the CTEQ5 parton distribution functions [25], and the attenuation of the fluxes assume Earth densities of the Preliminary Earth model described in Ref. [26]. As in Ref. [5], our upper bound of integration is 10^6 GeV because the attenuation of ν_τ fluxes at higher energies have not been evaluated, due to the complication of including tau energy loss at high energies [27]. Our results for the 100 TeV threshold are therefore conservative.

The ratio of the shower rate to the muon rate for the extragalactic flux models of Fig. 1 are used to bracket the theoretical expectations for the ratio in $2+2$ and $1+3$ mixing models, and compared with the standard model expectations. As in Ref. [5], we separate the flux models into two categories: more steeply falling fluxes (E^{-2}, ATM and the Mannheim AGN flux) and the less steep behavior of the other five sample fluxes of Fig. 1. Experimentally, the steeply falling fluxes and the models with a weaker energy dependence are characterized by distinct muon event rate nadir angle dependence and the threshold energy dependence. The two separate categories of fluxes, for threshold energies of 1, 10 and 100 TeV are shown in Figs. 2 (a-f). The $1+3$ models are bracketed

by the black lines, the $2+2$ models are represented by the shaded area and the standard model with the dark band.

For the 1 TeV threshold, the $1+3$ and $2+2$ event rates as a function of nadir angle overlap for both energy behaviors of the input fluxes. The no-oscillation band lies below the oscillation bands with the exception of the near horizontal rates in the steeply falling flux category (labeled E^{-2}). The separation between the oscillation and no-oscillation scenarios is better for higher thresholds, looking only in terms of the theoretical ratio of shower to muon event rates. However, the higher thresholds have lower event rates overall.

The bands in Fig. 2 indicate the different ratios for oscillation models relative to no-oscillation models, however, statistical errors from the signal as well as from the atmospheric background need to be included in order to interpret whether or not oscillation scenarios are distinguishable. In the next section, we include a discussion of statistical errors.

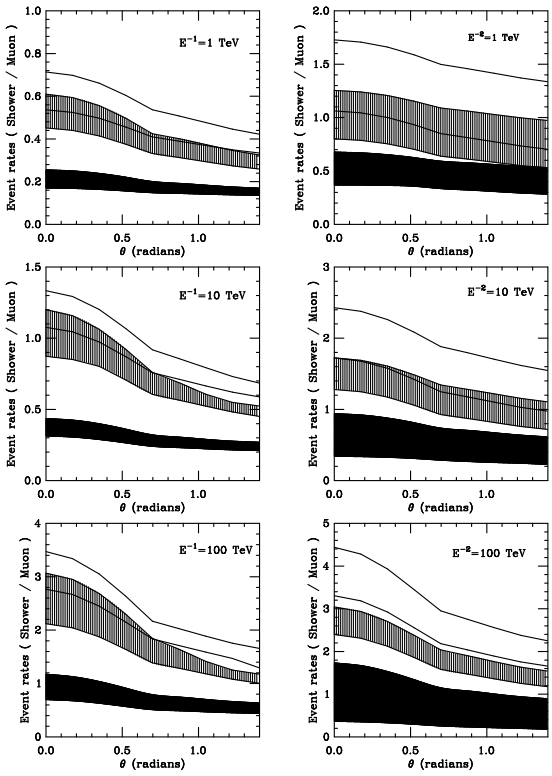

FIG. 2. Ratio of shower event rates to muon event rates for the $1+3$, $2+2$ and no oscillation scenarios as a function of nadir angles for threshold energies of 1 TeV, 10 TeV and 100 TeV, for the indicated fluxes. The black lines bracket the $1+3$ scenario, the shaded area represents the $2+2$ scenario and the dark band represents no-mixing case for the given fluxes.

IV. DISCUSSION

In Tables I-III we present our results for the shower and muon event rates integrated over the nadir angle for energy thresholds of 1 TeV, 10 TeV and 100 TeV and for a kilometer-size detector. The no-oscillation results agree with evaluations in Ref. [24] for fluxes in common, modulo corrections due to different parton distribution functions, a more precise evaluation of neutrino attenuation in the Earth [28] and the upper limit of energy integration. We do not include the topological defect models in these tables because the event rates are so low. For the 1 TeV threshold, only $0.1-0.2$ upward muon events are predicted per year for a km^2 instrumented area for the TD_WMB model. In all cases, we have considered shower rates in a km^3 volume, and muon rates/km^2. The two oscillation scenarios give the same muon event rates but very different shower rates. From Table I, we note that for 1 TeV energy threshold, atmospheric background is large.

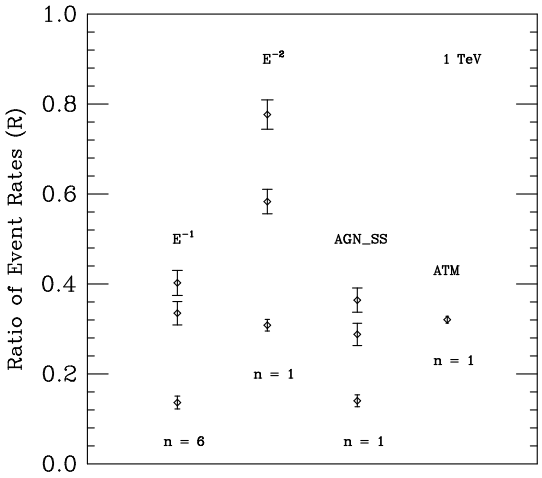

FIG. 3. Integrated over solid angle, the ratio of upward shower to muon event rates for given flux models for a threshold energy of 1 TeV. The error bars for $1+3$ scenario (top data), $2+2$ scenario (middle data), and no-mixing case (bottom data) are determined assuming n years of data taking.

In Figs. 3-5, we show the ratio R of the shower to muon event rates integrated over nadir angles ($R \equiv N_{shr}/N_\mu$) for energy thresholds of 1 TeV, 10 TeV and 100 TeV for a variety of fluxes and for different oscillation scenarios. The ratio of event rates in Figs. 3-5 have the atmospheric flux subtracted. The errors in the shower and muon rates (σ_{shr} and σ_μ) are evaluated with the assumption of a Poisson distribution, including the statistical error on the number of background events from the atmospheric flux. The error in the ratio of event rates is then given by,

$$\sigma_R = R\sqrt{\frac{\sigma_{shr}}{N_{shr}} + \frac{\sigma_\mu}{N_\mu}}\ . \tag{10}$$

The event rates N_{shr} and N_μ are from Tables I-III, scaled by n years as indicated in Figs. 3-5.

From Fig. 3 and Table I, we note that AGN fluxes, as well as E^{-2} and E^{-1} fluxes, would have the best possibility of separating different oscillation scenarios by detecting the showers and muons in kilometer-size detector over the period of one to six years, assuming a good understanding of the atmospheric muon neutrino and electron neutrino fluxes and normalizations near their current upper bounds. After one to six years of data taking, one would be able to separate oscillation from no oscillation scenario for the fluxes in Fig. 3. The GRB_WB flux would require more than twenty years of data to reduce statistical errors so that the error bars do not overlap for the two oscillation scenarios.

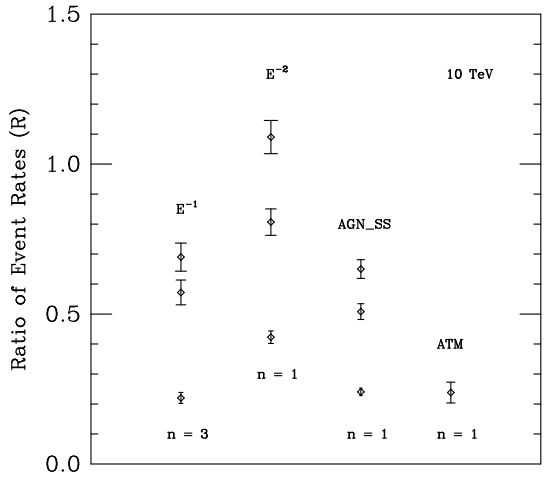

FIG. 4. Integrated over solid angle, the ratio of upward shower to muon event rates for given flux models for a threshold energy of 10 TeV.The error bars for $1+3$ scenario (top data), $2+2$ scenario (middle data), and no-mixing case (bottom data) are determined assuming n years of data taking.

The ratio of shower to muon event rates for an energy threshold of 10 TeV are shown in Fig. 4. As seen in Table II, the AGN model of Stecker and Salamon predicts large shower and muon rates, an order of magnitude larger than the atmospheric background. The AGN model of Mannheim and the GRB model of Waxman and Bahcall predict rates to be about 15-40% of the background, while E^{-2} and E^{-1} fluxes give significantly more events than the atmospheric background when oscillations are taken into account, assuming that the fluxes occur with a normalization at their current upper limit. Thus, there is a possibility of detecting extragalactic neutrinos by imposing a 10 TeV energy threshold [5]. We note that for the AGN_SS flux, as well as for E^{-1}, E^{-2} fluxes, one to three years would be sufficient to separate different oscillation scenarios. For the AGN_M95 and GRB_WB fluxes, it would be necessary to take data for seven to nine years respectively. The 10 TeV threshold is generally more favorable than the 1 TeV threshold because of the reduction of the atmospheric background and a sufficiently large signal.

If the energy threshold is increased to 100 TeV, the atmospheric background is small. The shower and muon event rates are several hundreds for AGN_SS model, while for all other models the rates are much smaller, but still significant, for kilometer-size detector in a time period of one year. Furthermore, the ratio of the shower and muon events can clearly separate oscillation and no-oscillation scenarios, as well as distinguish two oscillations scenarios that we consider. In Fig. 5 we show this ratio including statistical errors. We find that even with error bars it still seems possible to distinguish between different oscillation scenarios. However, in order to reduce statistical errors, the GRB_WB and AGN_M95 flux predictions would require collecting data for more than a decade. On the other hand, one year is sufficient for the AGN_SS flux. In the case of an E^{-1} flux, we expect several hundreds of showers and muons over the period of three years, which is necessary in order to reduce error bars to the point of being able to distinguish oscillation scenarios. For a steeper flux, E^{-2}, one year is sufficient to get enough events as well as to reduce the statistical errors at the current AMANDA limit on the isotropic flux normalization.

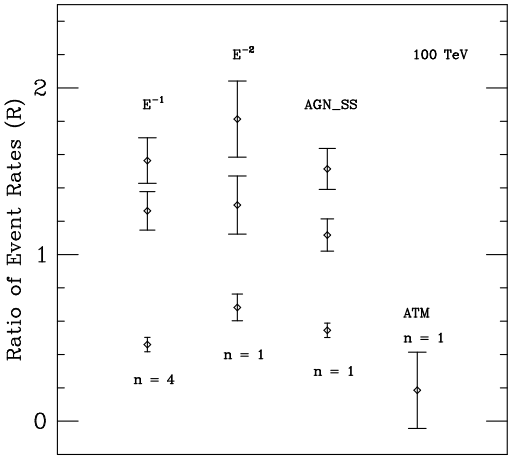

FIG. 5. Integrated over solid angle, the ratio of upward shower to muon event rates for given flux models for a threshold energy of 100 TeV. The error bars for $1+3$ scenario (top data), $2+2$ scenario (middle data), and no-mixing case (bottom data) are determined assuming n years of data taking.

Figs. 3-5 show the feature illustrated by Fig. 2, when

specific fluxes are integrated over nadir angle. Fluxes with similar spectra cluster with the same ratio, here, the Stecker-Salamon flux and E^{-1} have similar energy behaviors and similar ratios. Therefore, by using muon event energy and nadir angle dependence to characterize the energy spectrum of the incident flux, even without a detailed knowledge of the source of neutrinos, the ratio R will point to whether or not muon neutrinos mix with tau neutrinos in one of the two schemes described here.

The ratios in Figs. 3-5 differ for the different energy dependences of the fluxes for several reasons. The muon range increases with energy, so the muon event rates are sensitive to the energy dependence in a different way than the shower rates which have a constant volume factor. For less steep fluxes, *e.g.*, E^{-1} and AGN_SS, the high energy part of the spectrum gives a larger contribution to the muon rate than for fluxes with a steeper energy behavior, *e.g.*, E^{-2}. The ratio R of shower to muon event rates tends to increase with the steeper fluxes, and tends to increase with energy threshold. For all except the atmospheric flux, the electron neutrino contribution to the shower rate is substantial. The electron neutrino component of the atmospheric flux is small because of the high energies considered here, so the atmospheric ratio is not directly comparable to the ratios for other fluxes.

V. CONCLUSION

We have shown that measurements of the upward showers and muons, and considering their ratio, with the kilometer-size detector, could provide very good test of different oscillation scenarios. Taking into account statistical errors, we find that generic fluxes, such as $F^S_{\nu_\mu} = 10^{-12}\ (E/\mathrm{GeV})^{-1}\mathrm{GeV}^{-1}\mathrm{cm}^{-2}\mathrm{sr}^{-1}\mathrm{s}^{-1}$ and $F^S_{\nu_\mu} = 10^{-6}\ (E/\mathrm{GeV})^{-2}\mathrm{GeV}^{-1}\mathrm{cm}^{-2}\mathrm{sr}^{-1}\mathrm{s}^{-1}$, with energy threshold of 10 TeV and 100 TeV, would have enough statistics in one to four years of data taking to distinguish not only between oscillation and no oscillation scenario, but also whether it is 2+2 or 1+3 model. The AGN model of Stecker-Salamon [8], with a 10 TeV energy threshold predicts between 1200 and 2000 muons/km^2 per year and between 500 and 800 shower events/km^3 per year, with clear separation between different oscillation scenarios. The other AGN model, proposed by Mannheim [9], predicts less events and would require seven years to reduce statistical errors in the ratio of shower to muon event rates such that there is clear distinction between not only the no oscillation and oscillation cases, but also different oscillation models. If we want to use GRB_WB flux [10] to test these models, it would take nine years with the kilometer-size detector to get sufficient statistics. A higher energy threshold of 100 TeV makes the atmospheric neutrino background small, but event rates for extragalactic neutrinos are also reduced. Still, the AGN_SS model would be able to provide valuable information about the oscillation scenario, as well as E^{-2} flux in just one year of data, while an E^{-1} flux with our normalization would need four years. Other fluxes, such as GRB_WB and AGN_M95 flux would require much longer time.

The assumption of the existence of sterile neutrino is necessary to explain the solar, atmospheric, reactor and accelerator data. The MiniBooNE experiment [29] will search for $\nu_\mu \to \nu_e$ oscillations and test the LSND results. The presence of the sterile neutrino in the 2+2 model can be tested by the measurement of the suppression of NC/CC ratio of the solar neutrinos by the SNO experiment [30] whereas 1+3 model can be tested by searches from small amplitude oscillations at short baseline experiment such as ORLaND [31]. Since the 1+3 scenario at high neutrino energy mimics the three flavor bi-maximal mixing between $\nu_\mu \leftrightarrow \nu_\tau$, the results here can also be applied to three-flavor models.

Observation of the flavor ratio of extragalactic neutrinos could serve as a complementary test for oscillation models that incorporate sterile neutrinos. Oscillations of neutrinos from astronomical sources are averaged over very long baseline and thus cannot provide any direct information about the neutrino mass. However, we have shown that extragalactic neutrinos could be used to distinguish between different oscillation scenarios. The observed muon and shower event distributions as a function of angle and energy threshold will help determine the energy behavior of the incident extragalactic neutrino flux and point to a model or class of models for their sources. Combined measurements of the upward showers and muons and, in particular, their ratio provides a basic test of the oscillation scenario.

Acknowledgments

The work of S.I.D. and I.S. has been supported in part by the DOE under Contracts DE-FG02-95ER40906 and DE-FG03-93ER40792. The work of M.H.R. has been supported in part by National Science Foundation Grant No. PHY-9802403.

Note added:

After the submission of our paper, the SNO collaboration has reported their first results [32] which together with the SuperKamiokande results [1] favor oscillation into active flavors, however, given the theoretical and experimental uncertainties, oscillations into sterile neutrinos are still a possibility.

[1] Y. Suzuki, Nucl. Phys. Proc. Suppl. **91**, 29 (2001); B. T. Cleveland *et al.*, Nucl. Phys. Proc. Suppl. **38**, 47 (1995); J. N. Abdurashitov *et al.* [SAGE Collaboration], Phys. Rev. C **60**, 055801 (1999) [astro-ph/9907113];

T. A. Kirsten [GALLEX and GNO Collaborations], Nucl. Phys. Proc. Suppl. **77**, 26 (1999).
[2] Y. Fukuda *et al.* [Super-Kamiokande Collaboration], Phys. Rev. Lett. **81**, 1562 (1998) [hep-ex/9807003].
[3] C. Athanassopoulos *et al.* [LSND Collaboration], Phys. Rev. Lett. **81**, 1774 (1998) [nucl-ex/9709006]; C. Athanassopoulos *et al.* [LSND Collaboration], Phys. Rev. Lett. **77**, 3082 (1996) [nucl-ex/9605003]. I. Stancu [LSND Collaboration], Nucl. Phys. Proc. Suppl. **85**, 78 (2000).
[4] V. Barger, B. Kayser, J. Learned, T. Weiler and K. Whisnant, Phys. Lett. B **489**, 345 (2000) [hep-ph/0008019].
[5] S. Iyer Dutta, M. H. Reno and I. Sarcevic, Phys. Rev. D **62**, 123001 (2000) [hep-ph/0005310].
[6] D. V. Ahluwalia, C. A. Ortiz and G. Z. Adunas, hep-ph/0006092.
[7] H. Athar, M. Jezabek and O. Yasuda, Phys. Rev. D **62**, 103007 (2000) [hep-ph/0005104]. H. Athar, Astropart. Phys. **14**, 217 (2000) [hep-ph/0004191]. H. Athar, Nucl. Phys. Proc. Suppl. **87**, 442 (2000) [hep-ph/9912417].
[8] F. W. Stecker and M. H. Salamon, Space Sci. Rev. **75**, 341 (1996) [astro-ph/9501064].
[9] K. Mannheim, Astropart. Phys. **3**, 295 (1995).
[10] E. Waxman and J. Bahcall, Phys. Rev. D **59**, 023002 (1999) [hep-ph/9807282].
[11] G. Sigl, S. Lee, D. N. Schramm and P. Coppi, Phys. Lett. B **392**, 129 (1997) [astro-ph/9610221].
[12] U. F. Wichoski, J. H. MacGibbon and R. H. Brandenberger, hep-ph/9805419.
[13] E. Andres *et al.* [AMANDA Collaboration], Nucl. Phys. Proc. Suppl. **91**, 423 (2000) [astro-ph/0009242].
[14] P. Meszaros and E. Waxman, [astro-ph/0103275].
[15] E. Waxman and J. N. Bahcall, *Phys. Rev.* **D59**, 023002 (1999); J. N. Bahcall and E. Waxman, hep-ph/9902383; K. Mannheim, R. J. Protheroe and J. P. Rachen, Phys. Rev. D **63**, 023003 (2001) [astro-ph/9812398].
[16] V. Agrawal, T. K. Gaisser, P. Lipari and T. Stanev, Phys. Rev. D **53**, 1314 (1996) [hep-ph/9509423].
[17] T. K. Gaisser, *Cosmic Rays and Particle Physics* (Cambridge University Press, Cambridge, 1990).
[18] L. Pasquali, M. H. Reno and I. Sarcevic, Phys. Rev. D **59**, 034020 (1999) [hep-ph/9806428].
[19] G. Gelmini, P. Gondolo and G. Varieschi, Phys. Rev. D **61**, 036005 (2000) [hep-ph/9904457].
[20] P. Gondolo, G. Ingelman, M. Thunman and M. Thunman, Astropart. Phys. **5**, 309 (1996) [hep-ph/9505417].
[21] C. G. Costa, F. Halzen and C. Salles, hep-ph/0104039.
[22] F. Halzen and D. Saltzberg, Phys. Rev. Lett. **81**, 4305 (1998) [hep-ph/9804354]; S. Iyer, M. H. Reno and I. Sarcevic, Phys. Rev. D **61**, 053003 (2000) [hep-ph/9909393]; F. Becattini and S. Bottai, astro-ph/0003179.
[23] P. Lipari and T. Stanev, Phys. Rev. D **44**, 3543 (1991).
[24] See, for example, R. Gandhi, C. Quigg, M. H. Reno and I. Sarcevic, Phys. Rev. D **58**, 093009 (1998) [hep-ph/9807264];
R. Gandhi, C. Quigg, M. H. Reno and I. Sarcevic, Astropart. Phys. **5**, 81 (1996) [hep-ph/9512364].
[25] H. L. Lai *et al.* (CTEQ Collaboration), *Eur. Phys. J.* **C12**, 375 (2000).
[26] A. Dziewonski, Earth Structure, Global, in *Encyclopedia of Solid Earth Geophysics,* ed. David E. James (Van Nostrand Reinhold, New York).
[27] S. I. Dutta, M. H. Reno, I. Sarcevic and D. Seckel, Phys. Rev. D **63**, 094020 (2001) [hep-ph/0012350].
[28] V. A. Naumov and L. Perrone, Astropart. Phys. **10**, 239 (1999) [hep-ph/9804301].
[29] A. Bazarko [MiniBooNE Collaboration] Nucl. Phys. Proc. Suppl. **91**, 210-215 (2001) [hep-ex/0009056].
[30] A. McDonald [SNO Collaboration] Nucl. Phys. Proc. Suppl. **91**, 21-28 (2001) [hep-ex/0011025].
[31] F. Avignone [ORLaND Collaboration] Nucl. Phys. Proc. Suppl. **91**, 113-119 (2001) [hep-ex/0011025].
[32] Q.R. Ahmad *et al.* [SNO Collaboration] submitted to Phys. Rev. Lett. [nucl-ex/0106015].

TABLE I. Integrated upward shower (muon) rates per year for energy threshold of 1 TeV.

Model	E^{-1}	E^{-2}	AGN_SS	AGN_M95	GRB_WB	ATM
1+3	170(422)	2528(3255)	918(2521)	224(157)	26.9(65.8)	
2+2	141(422)	1898(3255)	726(2521)	163(157)	20.9(65.8)	
No osc	88.1(646)	1750(5676)	593(4228)	158(280)	18.3(113)	2355(7346)

TABLE II. Integrated upward shower (muon) rates per year for energy threshold of 10 TeV.

Model	E^{-1}	E^{-2}	AGN_SS	AGN_M95	GRB_WB	ATM
1+3	150(217)	954(875)	809(1245)	34.4(20.2)	21.3(28.4)	
2+2	124(217)	706(875)	633(1245)	24.5(20.2)	16.3(28.4)	
No osc	75.4(342)	652(1540)	514(2139)	24.4(36.3)	14.2(49.7)	58.5(246)

TABLE III. Integrated upward shower (muon) rates per year for energy threshold of 100 TeV.

Model	E^{-1}	E^{-2}	AGN_SS	AGN_M95	GRB_WB	ATM
1+3	84.8(54.2)	182(100)	386(255)	2.46(0.999)	7.28(4.03)	
2+2	68.4(54.2)	130(100)	285(255)	1.69(0.999)	5.21(4.03)	
No osc	42.0(91.3)	124(182)	251(460)	1.78(1.83)	4.99(7.31)	0.774(4.18)